Available online at www.sciencedirect.com
SCIENCE DIRECT®
Polymer 45 (2004) 3893–3900
polymer
www.elsevier.com/locate/polymer

Molecular dynamics simulation of oxygen diffusion in dry and water-containing poly(vinyl alcohol)☆

G.E. Karlsson, U.W. Gedde, M.S. Hedenqvist*

Department of Fibre and Polymer Technology, Royal Institute of Technology, SE-100 44 Stockholm, Sweden

Received 17 May 2003; received in revised form 2 December 2003; accepted 2 December 2003

Abstract

The kinetics and mechanisms of diffusion of oxygen and water in dry and water-containing amorphous syndiotactic poly(vinyl alcohol) were studied at 502 K and normal pressure by molecular dynamics simulation. Penetrant molecule trajectories were obtained in a system with 600 repeating units of poly(vinyl alcohol) and 0, 40 (2.6 wt%) and 80 (5.2 wt%) water molecules. Under dry conditions, oxygen molecules jumped in a cage-like fashion. The oxygen molecule diffused in a liquid-like fashion while water diffusion was cage-like in the system with 5.2 wt% water. The hydrogen bond lifetimes among the water molecules were significantly shorter than those formed between water and the polymer and between different polymer segments. The hydrogen bond lifetimes among all species were, within experimental error, unaffected by the content of water, even though the oxygen diffusivity increased exponentially and the water diffusivity increased to some extent with increasing water content. It seemed that the diffusivity was sensitive primarily to the decrease in concentration of polymer–polymer hydrogen bonds, which followed from the increase in water content. This finding was consonant with the analysis of the oxygen molecule motion relative to the nearest polymer backbone, which revealed that it jumped preferentially along the polymer chain and towards the backbone. This behavior was more pronounced when the dynamics were analyzed over longer distances (5 Å) and it was less pronounced in the water-rich systems. The simulations indicated that water clustering was absent and consequently that water was homogeneously distributed in the polymer systems.

Keywords: Molecular dynamics simulation; Poly(vinyl alcohol); Diffusion

1. Introduction

Dry poly(vinyl alcohol) (PVAL) has excellent barrier properties against permanent gases [1]. However, the barrier capacity of PVAL is greatly reduced under moist conditions [1]. This study addresses the question of why water has such a profound effect on the gas permeability of PVAL. The effect is commonly referred to as plasticization. One possibility is that water breaks strong hydrogen bonds established between the polymer molecules and that the penetrant molecules can diffusive more readily through the more loosely 'bonded' structure [2,3]. The details—how the water molecules are dispersed in the polymer; how the lifetime of the hydrogen bonds is affected by the presence of water; the character of the penetrant diffusion with respect to the polymer backbone in systems with different water contents—are still not fully understood. They have been thoroughly investigated in this study by means of a molecular dynamic (MD simulation.

The mechanisms of diffusion in polymers have been studied by MD simulations since the early 1990's. Tackeuchi et al. [4], for example, obtained reliable oxygen and nitrogen diffusivities in polyethylene. Boyd and co-workers studied diffusion of methane in several polymers [5]. Müller-Plathe [6,7] reported concentration-dependent water diffusivities in PVAL on systems with 3–100 vol% water. By studying mixtures of ethanol and water in the presence of PVAL, it was also found that PVAL is purely hydrophilic [8]. In a number of papers, Tamai et al. [9–13] reported MD simulations on PVAL hydrogels. They observed that the diffusion of oxygen and nitrogen increased with increasing water content [9]. They observed that these gases were located preferably in the first hydration shell

☆ Presented at 'Coupling Simulations and Experiments in Polymer Science: An International Symposium Honoring Professor Richard Boyd', Salt Lake City, Utah, USA, May 15–17, 2003.

* Corresponding author. Tel.: +46-8-790-7645; fax: +46-8-20-88-56.
E-mail address: mikaelhe@polymer.kth.se (M.S. Hedenqvist).

0032-3861/$ - see front matter © 2004 Elsevier Ltd. All rights reserved.
doi:10.1016/j.polymer.2003.12.082

next to the polymer chain at the lowest water content (~28 wt%). However, at the highest water content, the diffusing gases were mainly located outside the hydration shell. This paper reports the dynamics at low water contents (≤5.2 wt%), i.e. typical non-hydrogel situations.

Chassapis et al. [14] have developed tools for characterizing MD-generated small molecule trajectories in polymers by considering the penetrant path relative to the backbone of the polymer. Brandt [15], Dibenedetto [16] and Pace and Datyner [17–19] have also developed models for preferred paths of penetrant molecules. However, these models require the estimation of the energy associated with the bending of bundles of polymer chains as the penetrant molecule diffuses. Such input data are not required for MD simulation. In this work, the main objective is to reveal the diffusion mechanisms of oxygen in dry and swollen PVAL. The dependence on the water content of the oxygen diffusivity is quantified with MD simulation and the details of the motion of the oxygen molecules relative to the polymer backbones have been analyzed.

2. Experimental

2.1. Molecular dynamics simulation

The calculations were performed on SGI O2, SUN ULTRA ENTERPRISE 2 and PC (PIII) computers using a FORTRAN code originating from the group of Professor Richard Boyd of the University of Utah, Salt Lake City, USA. An all-*trans* syndiotactic PVAL chain with 600 repeating units was inserted in the simulation box and periodic boundary conditions were applied. The molecule system was allowed to densify and relax during a time period of several nanoseconds. The pressure during the equilibration was set to 0 atm and the temperature to 502 K. The constant bath method of Berendsen [20] was used to control pressure and temperature. The AMBER force field was used [21]. The usefulness of the AMBER force field in describing PVAL has been confirmed in a previous study of atactic PVAL [22]. The 6–12 (Lennard–Jones) and 10–12 (hydrogen bond) potentials were truncated at 9 Å with long-range corrections for energy and pressure. Coulombic interactions were considered according to Smith et al. [23], with the use of a switching function between 1.5 and 9 Å. The time step (t_s) was 0.5 fs and the equation of motion was integrated with the velocity-Verlet algorithm [24]. The two oxygen atoms were represented by a united atom with a hardcore diameter of 3.43 Å and a well depth of 940 J mol^{-1} [4]. The oxygen molecules were inserted in the dense system by continuously increasing their radius and well depth from zero to their final values. After the insertion, the system was allowed to relax for more than 1 ns. The same procedure was used for the insertion of the water molecules. Three systems were studied with, respectively 0, 40 and 80 water molecules, corresponding to the water concentrations 0, 2.6 and 5.2 wt%. Oxygen, water and backbone coordinates were sampled every 10th time step, i.e. every 5 fs.

2.2. Trajectories and chain orientation

A common way to characterize penetrant motion is by calculating the self-diffusivity (D_S) from the Einstein equation [9]:

$$r^2 = 6D_S t \tag{1}$$

where r^2 is the mean square displacement of the penetrant molecule and t is time. Eq. (1) can be rewritten in a more suitable form:

$$\langle |r_0(t_0 + t) - r_0(t_0)|^2 \rangle = 6D_S t \tag{2}$$

where t is the time from the start (t_0) and $\mathbf{r}_O$ are the vectors corresponding to the oxygen coordinates. Two different methods of analyzing the penetrant trajectories have been suggested. Pant et al. [25] used a time (τ) averaging of the penetrant position ($< \mathbf{r}_O(t) >_\tau$), to exclude non-diffusive motions. They used the squared distance (R_P^2) between two successive penetrant positions to characterize the penetrant motion:

$$R_P^2 = |\langle r_0(t + \tau) \rangle_\tau - -\langle r_0(t) \rangle_\tau|^2 \tag{3}$$

From the $R_P^2(t)$—time diagram, different types of penetrant motion can be distinguished. They are referred to as cage- and fluid-like motions. In cage-like motion, the penetrant is trapped for a long time in a 'cage' and a jump between cages is observed as a discrete event. In fluid-like motion, the penetrant tends to flow continuously with the motion of the matrix. Chassapis et al. [14] suggested a method by which the original trajectory is divided into equally long steps (λ) along the trajectory. This new trajectory is referred to as a 'reduced trajectory' and has the coordinates $\mathbf{r}_\lambda(n_\lambda)$, where n_λ is the successive number of the reduced trajectory coordinates:

$$|\mathbf{r}_0(t) - \mathbf{r}_\lambda(n_\lambda)| < \lambda \le |\mathbf{r}_0(t + t_s) - \mathbf{r}_\lambda(n_\lambda)|$$
$$= |\mathbf{r}_\lambda(n_\lambda + 1) - \mathbf{r}_\lambda(n_\lambda)| \tag{4}$$

where t_s is the time between coordinate samplings. The step length λ defines the number of reduced coordinates, and these should be less than the number of sampled points. Furthermore, Chassapis et al. [14] have developed methods to calculate the local chain orientation. We prefer to use a simpler method here, where the orientation of the polymer backbone is defined by three orthogonal vectors $\mathbf{n}_1$, $\mathbf{n}_2$ and $\mathbf{n}_3$ (Fig. 1(a)):

$$\mathbf{n}_1 = \frac{\mathbf{r}_k - \mathbf{r}_i}{|\mathbf{r}_k - \mathbf{r}_i|} \tag{5}$$

$$\mathbf{n}_2 = \frac{1/2(\mathbf{r}_k + \mathbf{r}_i) - \mathbf{r}_j}{|1/2(\mathbf{r}_k + \mathbf{r}_i) - \mathbf{r}_j|} \tag{6}$$

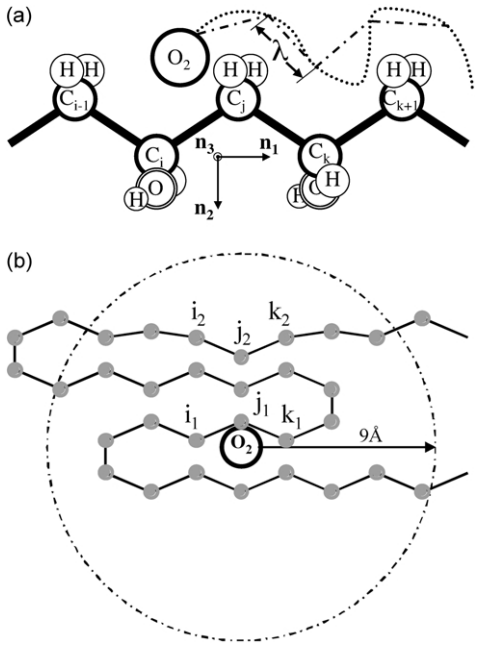

Fig. 1. (a) The backbone of PVAL and an O_2 penetrant molecule. The dotted line is the sampled penetrant trajectory and the dash-dotted line is a reduced trajectory with length λ. The backbone orientation vectors; $\mathbf{n}_1$, $\mathbf{n}_2$, and $\mathbf{n}_3$ are shown for the segment $C_i-C_j-C_k$. (b) The definition of the three nearest carbon contacts with the oxygen molecule.

$$\mathbf{n}_3 = \frac{\mathbf{n}_1 \times \mathbf{n}_2}{|\mathbf{n}_1 \times \mathbf{n}_2|} \tag{7}$$

where $\mathbf{r}_i$, $\mathbf{r}_j$ and $\mathbf{r}_k$ are the coordinates of carbon atoms i, j and k respectively. Carbon atom j is nearest to the penetrant oxygen molecule. Note that a contact established by 'chain folding', within a sphere with a radius of 9 Å, and the center on the oxygen molecule is not considered. Hence, the chain between the three contacts has to leave the sphere. This condition was used to minimize the effect of short kinks within the same chain on the calculations of the orientation of neighboring chains, and hence to exclude short range intramolecular orientational effects. The three nearest contacts (each contact is expressed in terms of three orthogonal vectors according to Fig. 1(a)) with the oxygen molecule, were defined according to Fig. 1(b). Correlations between the three sets of orthogonal vectors were sampled.

3. Results and discussion

The mean square displacement of the oxygen molecule as a function of time in the 5.2 wt% water system was non-linear with a maximum at 2000 ps and a minimum at 2800 ps (Fig. 2). The initial steep slope (≤2000 ps) was followed by a period with a less pronounced increase in the mean square displacement (2000–6000 ps). The irregular character of the curve at longer times (>6000 ps) was due to poor sampling statistics. The different slope coefficients can be understood by considering the jump map shown in

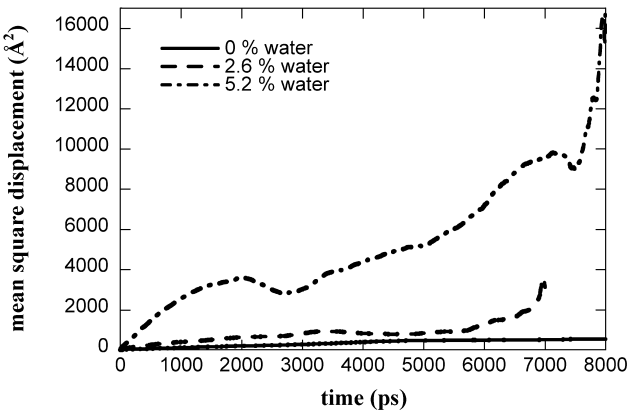

Fig. 2. Mean square displacements for oxygen molecules in PVAL at different water contents as shown in graph.

Fig. 3. Very long jumps ('spikes') were observed. The longest displacements over the 40 ps time period were more than 30 Å and a large number of jumps were in the range of 10–20 Å. Jumps in the range of 17–20 Å and longer occurred on average every 1000 ps. These extraordinarily long jumps affected the short-time statistics, giving rise to the initial steep slope in the mean square displacement time curve of the system with 5.2 wt% water (Fig. 2). It was first reasoned that these long jumps must have occurred in water-rich domains, similar to those that are observed in hydrogels [12,13]. Careful radial distribution function analysis, however, revealed that the water molecules were preferably located next to the polymer molecule and homogeneously distributed in the system. Thus there were no water-rich domains (clusters) in any of the systems. In addition, the radial distribution function showed that the spikes occurred in absence of neighboring water molecules. It seemed as if the absence of water triggered the large oxygen jumps through 'rigid' polymer segment regions once a channel developed. The spikes were larger in the 5.2 wt% water system than in the dry system, the explanation of which must be that the 'overall free volume' and mobility were larger in the former system. The spikes occurred both in the presence and in the absence of water in the 2.6 wt% system. The increase in local free volume associated with

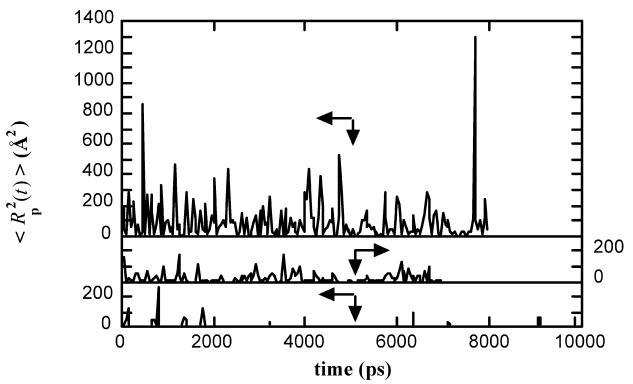

Fig. 3. Jump maps of oxygen molecules at 0 (bottom), 2.6 and 5.2 wt% (top) water. The time averaging was 40 ps.

water-polymer aggregates favored small oxygen jumps. The 'most frequently' observed distance between the water molecules as determined from the peak on the water–water radial distribution function was on the order of 8 Å for the 5.2 wt% water system and on the order of 9 and 10 Å for the 2.6 wt% water system. If one assumed a perfect cubically arranged water lattice, the closest distance between the water molecules would be 9 and 10 Å respectively. This is in good agreement with the radial distribution function, which dropped rapidly for distances below 8.5 and 9 for the 5.2 and 2.6 wt% systems respectively. The longest oxygen jumps, corresponding to the spikes in the jump map, were on the order of 10–14 Å in the 2.6 wt% and as high as 35 Å in the 5.2 wt% system. Thus the longest jumps were longer than the water-to-water distances discussed above. However this does not imply that the oxygen must have meet one or several water molecules during these jumps, since the water-to-water distances were averaged over long periods of time. The reason why diffusion spikes occurred preferentially in dry regions in the 5.2 wt% system but in both dry and wet regions in the 2.6 wt% system is not clear. It may only be speculated upon, but the fact that the degree of swelling (volume increase) was substantially larger in the 5.2 wt% system may leave room for occasional oxygen transport in 'dry regions'. The incorporation of 2.6 and 5.2 wt% water led to an 8 and 38% increase in box volume.

The mean square displacement over a longer time period, still within the limit of sufficient statistics, was less influenced by the long jumps and a more reliable statistical mean was obtained. Fig. 4 shows the oxygen diffusivity in PVAL as a function of the water content. For the systems with 0 and 2.6 wt% water only one data point was obtained for each system, whereas for the system with 5.2 wt%, a value was obtained based on the slope coefficient for the data between 200 and 800 ps ($D = 4.3 \times 10^{-5}$ cm^2 s^{-1}) and another value was established on the basis of the data obtained between 3500 and 5000 ps ($D = 1.8 \times 10^{-5}$ cm^2 s^{-1}). The latter value essentially probes the penetrant motion between 200 and 5000 ps. To our knowledge, no data have been reported for the oxygen diffusivity of PVAL at ~500 K and in this particular water concentration range (0–5 wt%). Tamai et al. [9] reported an oxygen diffusivity of approximately 5×10^{-7} cm^2 s^{-1} at 300 K and 27.5 vol% water. It is, however, difficult to compare their results with the data obtained in this paper due to the large differences in temperature and solute concentration. A very important feature is that the logarithm of the oxygen diffusivity is proportional to the water concentration (Fig. 4), which is in agreement with the semi-empirical equation [26]:

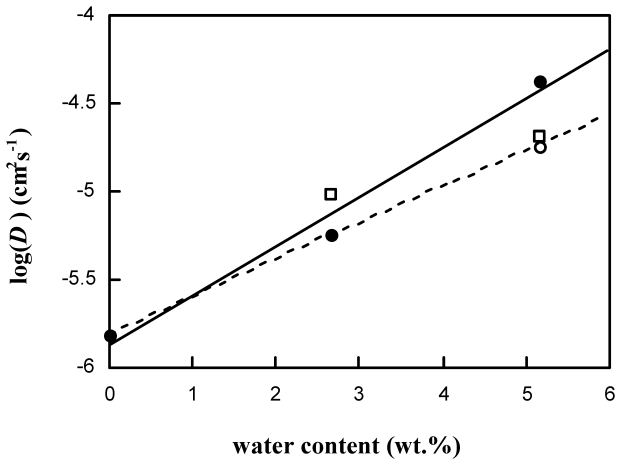

Fig. 4. Diffusion coefficient as a function of water concentration determined from the slope of mean square displacement vs. time: (●) oxygen, calculated between 200 and 800 ps, (○) oxygen, calculated between 3500 and 5000 ps, (□) water. The solid and dashed lines are the least squares fits of Eq. (8) to, respectively, the (●) and (○) values.

$$D = D_{C0} \times \exp(\gamma C_w) \quad (8)$$

where γ is a parameter that quantifies the increase in diffusivity due to the presence of the solute, C_w is the water concentration and D_{C0} is the diffusivity at $C_w = 0$. Fitting of Eq. (8) to the data obtained by simulation yielded the following parameter values: $D_{C0} = 1.5 \times 10^{-6}$ cm^2 s^{-1} and $\gamma = 0.48$ (1/wt%). It should be noted that the diffusivity data point obtained from short term penetrant displacement in the system with 5.2 wt% water is off the regression line by half an order of magnitude in diffusivity (Fig. 4). The Cohen–Turnbull free volume theory [27] was not capable of describing the simulated data. The theoretical curve showed a negative curvature at higher water concentration which clearly deviated from the linear trend in the log(diffusivity) − water concentration data shown in Fig. 4. This finding substantiates the idea proposed by Kulkarni and Stern [28] that the free-volume approach is not suitable for systems with strong intermolecular interactions.

Water diffusivities were also obtained from 200 ps trajectories: 9.5×10^{-6} cm^2 s^{-1} (2.6 wt% water) and 2.1×10^{-5} cm^2 s^{-1} (5.2 wt% water). These values were lower than the water zero-concentration diffusivities for atactic PVAL obtained both experimentally and by MD simulation previously reported by Karlsson et al. [22]. The deviation was unexpected but it may have been because the size of the previous system was smaller and the present system contained syndiotactic rather than atactic PVAL. However, the values reported for syndiotactic PVAL were in accordance with data presented by Müller-Plathe [7], who reported a water diffusivity in PVAL of 3.0×10^{-7} cm^2 s^{-1} at 375 K at 4 vol% water. This value may be compared with our data at 502 K by extrapolating their data with an activation energy of 50 kJ mol^{-1} [29]. This yielded $D = 1.7 \times 10^{-5}$ cm^2 s which is in the same range as our data.

The small difference in the diffusivities of water and oxygen is also interesting considering the difference in their sizes (Fig. 4). Whereas the 'effective' molecular diameter of water is larger than that of oxygen [30], the 'van der Waal' based molecular diameters are almost the same and the 'gas-viscosity' molecular diameter of water is smaller than that of oxygen [31]. In our case with the large number of hydrogen bonds it would be expected that the 'effective'

larger size of water would prevail. However it seemed that the relative sizes of the penetrants were less important and that the rate of diffusion was determined mainly by the hydrogen bonds between the polymer chain segments; a finding observed already for water diffusion in dry PVAL [22].

Fig. 3 shows jump maps (Eq. (3) describes the mathematical formalism), using a 40 ps averaging time for the position of the oxygen molecule in the three systems studied. The dry system exhibited cage-like diffusion with well-resolved discrete jumps of the oxygen molecule. Most of the time, the oxygen molecule was trapped and vibrated in the same cage. The O_2 jump map in the system with 5.2 wt% water showed liquid-like diffusion, i.e. the penetrant 'flowed' with the moving polymer chain segments. The O_2 jump map for the system with an intermediate water concentration (2.6 wt%) can be described as a combination of cage-like and liquid-like diffusion.

Fig. 5 shows the jump map for the water molecules. The jump maps, constructed on the basis of the average position of a water molecule during 40 ps, were constructed from the water molecule trajectories during 200 ps in the systems with 2.6 and 5.2 wt% water. The jump maps shows clearly that water diffused in a cage-like fashion even at the highest water concentration. The stronger interaction between penetrant and polymer and between different penetrant molecules more efficiently prohibits continuous flow of the water penetrant in the system with 5.2 wt% in contrast the case of O_2 as the penetrant molecule. Interestingly, the spikes observed in the oxygen jump-map, and attributed to water-free regions, were also observed for water in both systems. Also for water, these jumps possibly occurred in the absence of other water molecules. This is consonant with the view that the water molecules are evenly distributed along the polymer backbone and that no large clusters occur.

The backbone orientation was calculated for the $\mathbf{n}_l$ direction as the absolute value of the cosine of the angle (ϕ_{ij}) between the vectors $\mathbf{n}_{l,ib}$ and $\mathbf{n}_{l,jb}$ ($ib > jb$, $1 \leq ib$, $jb \leq 3$), where the indices ib and jb correspond to the backbone segment nearest ($ib = 1$), second nearest ($ib = 2$), and third nearest ($ib = 3$) to the oxygen molecule. The orientation ($< |\cos \phi_{ib,jb}| >$) was approximately 0.71–0.78 for all combinations of ib and jb in the three systems, but it showed a slight tendency to increase in the systems with a higher water concentration (Table 1). The chains tended to lie in parallel bundles in the vicinity of the diffusing oxygen molecule, which was also assumed in the derivations of the diffusion theories of Brandt [15], Dibenedetto [16] and Pace et al. [17].

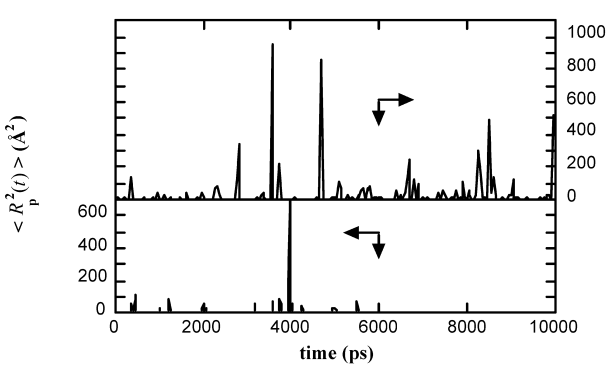

Fig. 5. Jump maps of water molecules at 2.6 (bottom), and 5.2 wt% (top) water. The time averaging was 40 ps.

The angles ($\Theta_{i,\lambda}$) between the backbone vectors ($\mathbf{n}_1$, $\mathbf{n}_2$ and $\mathbf{n}_3$) nearest to the oxygen molecule and the first step of the reduced trajectory:

$$\cos \Theta_{i,\lambda} = \frac{\mathbf{n}_i \cdot \mathbf{r}_\lambda}{|\mathbf{n}_i| \cdot |\mathbf{r}_\lambda|} \tag{9}$$

was calculated for four different step lengths of the reduced trajectory: $\lambda = 0.625$, 1.25, 2.5 and 5 Å. The index m corresponds to the orientation direction and λ is the step length of the reduced trajectory. Fig. 6(a)–(c) show the probability density function, p ($\cos \Theta_{i,\lambda}$) for the three systems with different water contents. The direction of the short penetrant displacements ($\lambda = 0.625$ Å) was completely uncorrelated with $\mathbf{n}_l$ (vector parallel to the backbone, see Fig. 1(a)) as is obvious from the flat almost horizontal p distribution (Fig. 6(a)). The longer penetrant displacements ($\lambda \geqq 2.5$ and 5 Å) were preferentially along $\mathbf{n}_l$, which is demonstrated by the higher p values at $\cos \Theta_{i,\lambda}$ near -1 and $+1$ (examples illustrated by the bold arrows in Fig. 6(a)). This correlation between penetrant trajectory and $\mathbf{n}_l$ was most pronounced in the dry system but it was also detectable in both water-containing systems.

Fig. 6(b) shows that the displacement of the oxygen molecule is preferentially towards the polymer backbone, as indicated by the decrease in p when going from $\cos \Theta_{i,\lambda} = -1$ to $\cos \Theta_{i,\lambda} = +1$. Thus the preferred direction of λ is at 180° angle to $\mathbf{n}_2$ (Fig. 1(a)). This trend was the same for all studied λ and in all the studied systems, independent of water content.

The penetrant molecule trajectory with reference to $\mathbf{n}_3$ showed a very pronounced dependence on the water content (Fig. 6(c)). The jumps showed no correlation with $\mathbf{n}_3$ in the systems with 5.2 wt% water (flat almost horizontal p distribution). However, in the system with 2.6 wt% water ($\lambda = 5$ Å), the oxygen molecule preferred to move perpendicular to the polymer backbone (as indicated by the bold arrow in Fig. 6(c)). Interestingly the shoulders located at intermediate values of $\cos \Theta_{3,5\ Å}$ in the systems with 0 and 2.6 wt% water were in accordance with the data shown in

Table 1
Orientation of the polymer backbone segments near an oxygen molecule

Water concentration (wt%)	$\langle \lvert\cos \phi_{1,2}\rvert \rangle$	$\langle \lvert\cos \phi_{1,3}\rvert \rangle$	$\langle \lvert\cos \phi_{2,3}\rvert \rangle$
0	0.715	0.714	0.731
2.6	0.778	0.769	0.763
5.2	0.761	0.758	0.758

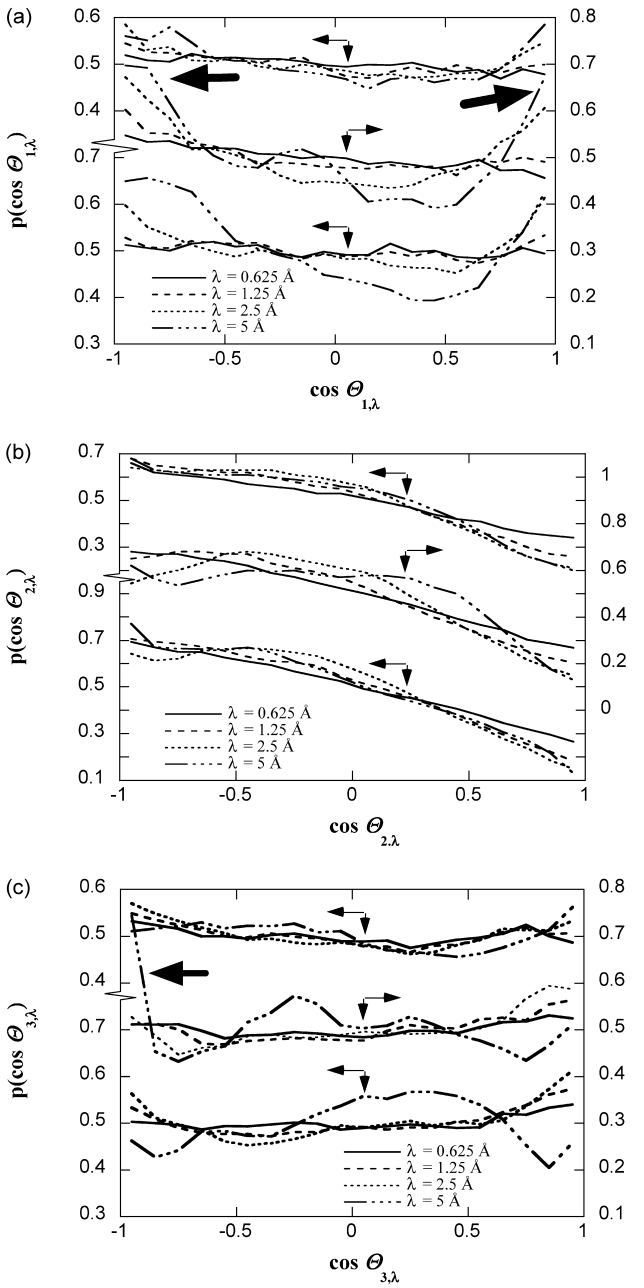

Fig. 6. (a) The angle between $\mathbf{n}_1$ and the reduced oxygen trajectories for different λ and water contents. The three sets of four curves correspond, from bottom to top, to 0, 2.6 and 5.2 wt% water. The bold arrows are explained in the text. (b) The angle between $\mathbf{n}_2$ and the reduced oxygen trajectories for different λ and water contents. The three sets of four curves correspond, from bottom to top, to 0, 2.6 and 5.2 wt% water. (c) The angle between $\mathbf{n}_3$ and the reduced oxygen trajectories for different λ and water contents. The three sets of four curves correspond, from bottom to top, to 0, 2.6 and 5.2 wt% water. The bold arrow is explained in the text.

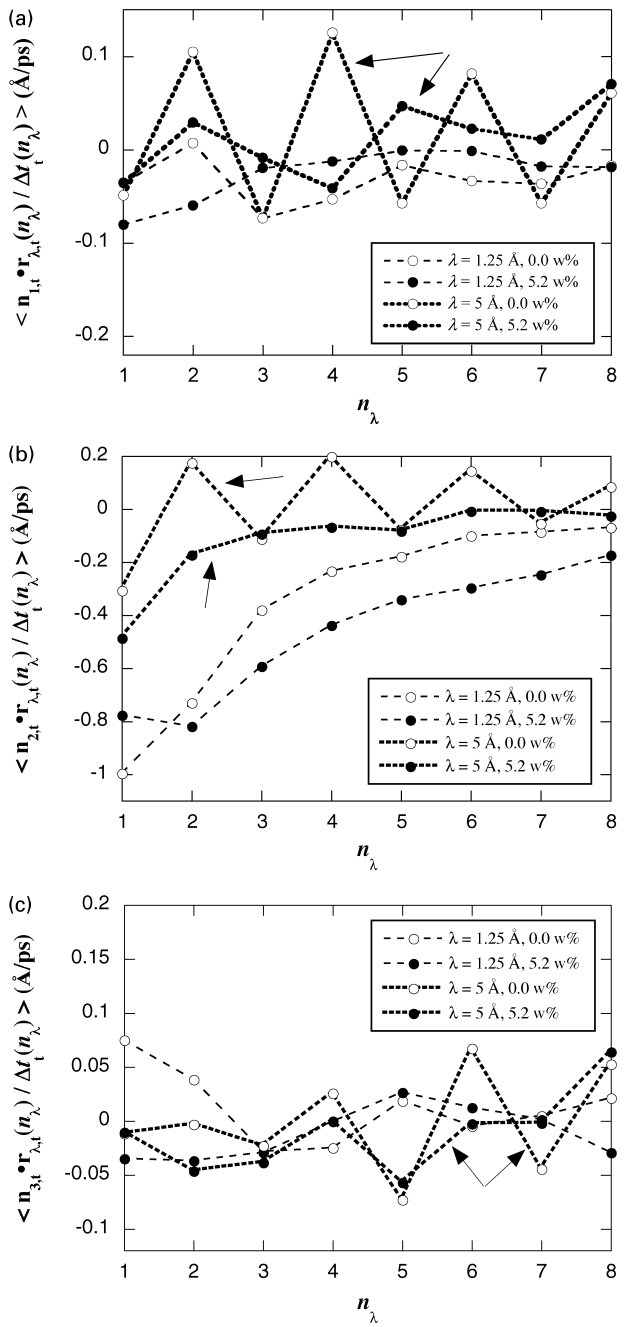

Fig. 7. (a) The velocity of the oxygen molecule obtained from the reduced trajectory projected along $\mathbf{n}_1$ averaged over 1 to 8 consecutive steps. The arrows are explained in the text. (b) The velocity of the oxygen molecule obtained from the reduced trajectory projected along $\mathbf{n}_2$ averaged over 1 to 8 consecutive steps. The arrows are explained in the text. (c) The velocity of the oxygen molecule obtained from the reduced trajectory projected along $\mathbf{n}_3$ averaged over 1 to 8 consecutive steps. The arrows are explained in the text.

Fig. 6(a) and (b). In conclusion, based on the analysis between the oxygen molecule and its nearest polymer chain neighboring segment, the oxygen molecule preferred to move along the chain and towards the nearest chain backbone, especially when longer penetrant molecule displacements (~5 Å) were considered. This tendency decreased with increasing water content. The tendency for the oxygen molecule to move towards the chain axis is probably a consequence of the fact that it favors increased molecular close packing. The tendency was indeed an average event and, of-course, all kinds of jump directions were observed.

Fig. 7(a)–(c) show the oxygen velocity obtained from its reduced trajectory projected in the *n*-directions given in Fig. 1. At time *t*, the backbone orientation was calculated and the reduced trajectory was started. It included 8 ($n_\lambda = 1, 2 \ldots 8$) steps with step lengths (λ) of 1.25 and 5 Å. Thus the velocity orientation function was averaged over 1 to 8 steps. Each pair of reduced trajectory coordinates was associated with a time $\Delta t_i(n_\lambda)$ interval from which the velocity was calculated. All available starting points were used, i.e. those collected every 10th time step. Fig. 7(a) shows the velocities projected along $\mathbf{n}_1$. For clarity the 2.6 wt% data were not shown in any of Fig. 7(a)–(c). The velocities of $\lambda = 1.25$ Å relaxed more rapidly than the velocities of $\lambda =$ 5 Å, as observed by smoother curves leveling out towards zero at higher n_λ (Fig. 7(a)). The 'saw-tooth' behavior of the $\lambda = 5$ Å data clearly shows that the oxygen molecule moved back and forth. This tendency decreased with increasing water content, as indicated by the arrows. The velocities projected along $\mathbf{n}_2$ relaxed more slowly than the velocities projected along $\mathbf{n}_1$, as indicated by the slower approach of the different curves towards zero at higher n_λ (Fig. 7(a) and (b)). For the trajectory with $\lambda = 5$ Å, the velocities in the systems with 0 and 2.6 wt% water showed saw-tooth curves (cage-like diffusion). The systems with 5.2 wt% water lacked the saw-tooth curves, i.e. they exhibited liquid-like diffusion (compare the curves indicated by arrows). These data are in accordance with the corresponding jump maps (Fig. 3). The cage-like features were also present for $\lambda = 5$ Å in the velocities projected along $\mathbf{n}_3$ of the systems with $\leq$2.6 wt% water (observe the 0 wt% curves in Fig. 7(c)). The liquid-like nature of oxygen diffusion in the system with 5.2 wt% water was also confirmed in this case (Compare the curves indicated by arrows in Fig. 7(c)).

The hydrogen bond lifetimes are displayed in Table 2. To obtain sufficient statistics, a hydrogen bond was considered to exist when the hydrogen–oxygen distance was shorter than 3 Å. A distance of 2.5 Å was chosen for the polymer–polymer interactions. This did not change the trend but merely increased the lifetime (Table 2). The lifetimes of the polymer–polymer and water†polymer hydrogen bonds were the same and insensitive to the actual water content. The water–water hydrogen bond lifetimes were significantly shorter than those were the polymer was involved. This is consonant with the finding of Tamai and Tanaka [9] who observed that the water mobility in hydrogels was significantly reduced in the vicinity of the polymer. The fact that the hydrogen bond lifetimes were independent of water content was somewhat surprising, since the oxygen diffusivity, and to some extent also the water diffusivity, increased substantially with increasing water content. In order to see whether the number of hydrogen bonds was the key issue rather than the average lifetime, the total hydrogen bond lifetime density within a 200 ps simulation was calculated. As the sum of the total number of the different hydrogen bonds multiplied by their average lifetimes and divided by the box volume. The values were 2 ns/nm^3 (0 wt% water), 2.5 (2.6 wt%) and 2.2 (5.2 wt%). Thus the increase in diffusivity could not be explained either by a decrease in total number of hydrogen bonds or by a decrease of their respective lifetimes. However the concentration of polymer–polymer hydrogen bonds decreased to 85% (2.6 wt% water) and 53% (5.2 wt%) of that of the dry system. It thus seems reasonable to conclude that the oxygen diffusivity and perhaps also the water diffusivity depended uniquely on the number of hydrogen bonds between the polymer segments. This seems even more reasonable when considering the above analysis of the oxygen motion relative to the polymer backbone. As shown previously, the oxygen molecule tended to move along the polymer chain and towards the chain backbone. Such motion must have been particularly sensitive to the number of polymer–polymer hydrogen bonds and only partly to the water–polymer and water–water bonds.

Table 2
Hydrogen bond lifetimes

Water concentration (wt%)	τ_{PP}[a] (fs)	τ_{PP}[b] (fs)	τ_{PW}[b] (fs)	τ_{WW}[b] (fs)
0	104 (±80)	77 (±60)	–	–
2.6	103 (±80)	74 (±45)	76 (±28)	28 (±11)
5.2	98 (±66)	74 (±38)	81 (±32)	23 (±6)

[a] Hydrogen bond lifetime defined as the time when the hydrogen and oxygen atoms were within a distance of 2.5 Å. No angular restriction. PP = polymer–polymer hydrogen bond.

[b] Hydrogen bond lifetime defined as the time when the hydrogen and oxygen atoms were within a distance of 3 Å. No angular restriction. Hydrogen bonds between polymer and polymer (PP), polymer and water (PW) and water and water (WW).

4. Conclusions

Water was uniformly distributed in PVAL and the water–polymer hydrogen bond lifetimes were significantly smaller than those between water and polymer and polymer and polymer. The hydrogen bond lifetimes remained the same despite the fact that the oxygen diffusivity, and to some extent also that of water, increased substantially with increasing water content. It seemed that the diffusivities were primarily dependent on the number of hydrogen bonds between polymer segments, probably because the oxygen molecule was moving preferentially along the polymer chain and towards the backbone, the analysis based on its interactions with the nearest polymer chain neighboring segment. These trends were more pronounced in the dry system. Occasional very large displacements of oxygen were found to occur in the absence of neighboring water. The velocities of the reduced trajectory and the jump maps showed that oxygen diffusion in the systems with low water content ($\leq$2.6 wt%) occurred by occasional jumps between free volume sites ('cages'), in which the penetrant

molecules were trapped for a relatively long period of time. However, in the system with 5.2 wt%, water diffusion was more liquid-like with less well time-resolved displacements. Water diffusion was always cage-like.

Acknowledgements

We thank Professor R.H. Boyd, University of Utah, USA for providing the molecular dynamics simulation software. The financial supported from the Swedish Research Council of Engineering Sciences (TFR, VR; grant: 97-125 doss 210) and National Graduate School in Scientific Computing (NGSSC; grant 200-97-24) is gratefully acknowledged.

References

[1] Robertson GL. Food packaging, principles and practise. New York: Marcel Dekker; 1993.
[2] Náray-Szabó G. In: Scheiner S, editor. Molecular interactions, from van der waals to strongly bound complexes. New York: Wiley; 1997.
[3] Hertz HG. In: Hadzi D, editor. Theoretical treatments of hydrogen bonding. New York: Wiley; 1997.
[4] Takeuchi H, Okazaki K. J Chem Phys 1990;92:5643.
[5] Boyd RH. Trends Polym Sci 1996;4:12.
[6] Müller-Plathe F. J Membr Sci 1998;141:147.
[7] Müller-Plathe F. J Chem Phys 1998;108:8252.
[8] Müller-Plathe F, van Gunsteren WF. Polymer 1997;38:2259.
[9] Tamai Y, Tanaka H. Fluid Phase Equilib 1998;144:441.
[10] Tamai Y, Tanaka H. Chem Phys Lett 1998;285:127.
[11] Tamai Y, Tanaka H. Phys Rev E 1999;59:5647.
[12] Tamai Y, Tanaka H, Nakanishi K. Macromolecules 1996;29:6750.
[13] Tamai Y, Tanaka H, Nakanishi K. Macromolecules 1996;29:6761.
[14] Chassapis CS, Petrou JK, Petropoulos JH, Theodorou DN. Macromolecules 1996;29:3615.
[15] Brandt WW. J Phys Chem 1959;63:1080.
[16] Dibenedetto AT. J Polym Sci Part A 1963;1:3459.
[17] Pace RJ, Datyner A. J Polym Sci Polym Phys Ed 1979;17:437.
[18] Pace RJ, Datyner A. J Polym Sci Polym Phys Ed 1979;17:453.
[19] Pace RJ, Datyner A. J Polym Sci Polym Phys Ed 1979;17:465.
[20] Berendsen HJC, Postma JPM, van Gunsteren WF, DiNola A, Haak JR. J Chem Phys 1984;81:3684.
[21] Weiner SJ, Kollman PA, Case DA, Singh UC, Ghio C, Alagona G, Profetia Jr, S, Weiner P. J Am Chem Soc 1984;106:765.
[22] Karlsson GE, Johansson TS, Gedde UW, Hedenqvist MS. J Macromol Sci-Phys 2002;B41:185.
[23] Smith GD, Jaffe RL, Yoon DY. Macromolecules 1993;26:298.
[24] Swope WC, Andersen HC, Berens PH, Wilson KR. J Chem Phys 1982;76:637.
[25] Pant PVK, Boyd RH. Macromolecules 1993;26:679.
[26] Vieth WR. Diffusion in and through polymers. Munich: Hanser Verlag; 1991.
[27] Neway B, Hedenqvist MS, Mathot VBF, Gedde UW. Polymer 2001; 42:5307.
[28] Kulkarni SS, Stern SA. J Polym Sci Polym Phys Ed 1983;21:441.
[29] Crank J, Park GS. Diffusion in polymers. London: Academic Press; 1968.
[30] Krevelen DWv. Properties of polymers. Amsterdam: Elsevier; 1976.
[31] Moore WJ. Physical chemistry. Englewood Cliffs: Prentice-Hall Inc; 1972.